Fragile magnetic ordering between robust 2D-ferrimagnets in the AFe 3 (SeO 3) 2 F 6 (A=K, Rb, Cs) series

Haoming Yang, Olivier Mentré, Tianyu Zhu, Claire Minaud, Clemens Ritter, Xinan Zhang, Yong Jin, Minfeng Lü

▶ **To cite this version:**

Haoming Yang, Olivier Mentré, Tianyu Zhu, Claire Minaud, Clemens Ritter, et al.. Fragile magnetic ordering between robust 2D-ferrimagnets in the AFe 3 (SeO 3) 2 F 6 (A=K, Rb, Cs) series. Journal of Materials Chemistry C, 2022, 10 (6), pp.2139-2148. 10.1039/D1TC05650F . hal-03870715

HAL Id: hal-03870715
https://hal.science/hal-03870715v1

Submitted on 24 Nov 2022

HAL is a multi-disciplinary open access archive for the deposit and dissemination of scientific research documents, whether they are published or not. The documents may come from teaching and research institutions in France or abroad, or from public or private research centers.

L'archive ouverte pluridisciplinaire **HAL**, est destinée au dépôt et à la diffusion de documents scientifiques de niveau recherche, publiés ou non, émanant des établissements d'enseignement et de recherche français ou étrangers, des laboratoires publics ou privés.

ARTICLE

Fragile magnetic ordering between robust 2D-ferrimagnets in the $AFe_3(SeO_3)_2F_6$ (A=K, Rb, Cs) series

Received 00th January 20xx,
Accepted 00th January 20xx

DOI: 10.1039/x0xx00000x

Haoming Yang,[a] Olivier Mentré,[b,*] Tianyu Zhu, [a] Claire Minaud,[b] Clemens Ritter,[c] Xinan Zhang,[a] Yong Jin,[a] and Minfeng Lü,[a,†]

Mixed anion compounds $AFe_3(SeO_3)_2F_6$ (A=K, Rb) have been synthesized by hydrothermal reactions. Prior results obtained for the isostructural Cs analog have revealed original 2D-ferrimagnetic (FI) blocks, antiferromagnetically (AFM) ordered around ~120 K. Surprisingly, the whole series orders at a nearly constant T_N temperature with similar field-induced magnetization steps, despite significant changes of the interlayer thickness. The metamagnetic transition from AFM to FI on oriented single crystals and Cp measurements prove an in-plane easy-magnetic axis confirmed by neutron powder diffraction (NPD). The ferrimagnetic alignment [Fe(1)↑−Fe(2)↓−Fe(1)↑] in each 2D subunit is robust, but the AFM-ordering between them is broken under weak field leaving field-aligned 2D-macrospins, with weak magnetocrystalline anisotropy. DFT+U calculations validate the exchange ratio J_{inter}/J_{intra} of ~5.10^{-3} for all compounds and the relatively high T_N value is well predicted by a modified random-phase approximation (RPA) like relation, established for Quasi-Low-Dimensional Heisenberg Antiferromagnets. However, our calculations of intralayer magnetic dipole-dipole (MDD) interactions indicate a non-neglectable values and suggest the latter to assist the in-plane spin orientation below T_N. At T_N, under field a 3D-Heisenberg model was deduced for the AFM →FI transition from the critical behavior using modified Arrott plots.

Introduction

Besides the well-known eleven bidimensional (2D) Archimedean tilings in which all vertices are equivalent ,[1] there has been intensive search on the magnetism of more complex lattices, extending the dimensionality from 1D to 3D. It gives rise to exotic magnetic states and a variety of critical points. In the 3D cases, one good example concerns the 3D- frustrated pyrochlore lattice which can lead to the emergence of spin-ice fundamental states, such as found in $Ln_2Ti_2O_7$ compounds.[2] Although the theory on incrementally complex lattices is developed with application of various parameters, such as moment values (and quantum versus classical spins), magnetic anisotropy etc .., the realization of specific lattices in real materials is often challenging. Recently, *Lu* and *Kageyama* have prepared the perfect emulation of the so-called 2D-cubic tiling of S=5/2 spins in the $CsFe_3(SeO_3)_2F_6$ inorganic mixed anion compound.[3] Although built on three staggered layers of Fe^{3+} ions arranged in isolated blocks, the projection perpendicular to the stacking axis corresponds perfectly to the in-planar representation of the cubic-tilling, as shown Figure 1. Indeed, the experimental characterization of $CsFe_3(SeO_3)_2F_6$ suggests a ferrimagnetic (FI) ordering within the 2D cube-tiles, similar to what has been theoretically predicted for this lattice with S=1/2, obtained as one of the variants after distortion of the triangular lattice. [3] Despite the absence of significant magnetic exchange paths between individual 2D-lattices in the $CsFe_3(SeO_3)_2F_6$, 3D antiferromagnetic ordering was observed below T_N~120K, easily broken into a field-induced ferrimagnetic state at relatively low field (μ_0.H<1T). Such "high" T_N in a system built on mainly uncoupled FI 2D-subunits is somewhat intriguing. Here we prepared and characterized the A= K and Rb analogs and investigate the full series on the basis of neutron powder diffraction (NPD), anisotropic magnetic measurements using oriented single crystals, heat capacity DFT+U and magnetic dipole-dipole (MDD) interactions calculations,. We paid special attention to the ingredients driving the metamagnetic transition, returning a common model valid for the full series.

Experimental

Synthetic procedures

Reagents:$FeCl_2$•$4H_2O$ (Acros Organics, 99%), HF (Energy Chemical, 48%-55% wt in H_2O), KOH (11M) RbOH (Alfa Aesar, 50% w/w), and SeO_2 (Alfa Aesar, 99.4%) were used as received.

$KFe_3(SeO_3)_2F_6$: Hexagonal shaped crystals were obtained from the hydrothermal reactions. A stoichiometric of KOH / $FeCl_2$•$4H_2O$ /SeO_2 with the molar ratio of 1:1:3 (1 mmol of KOH(0.096 ml), 1 mmol (0.1988 g) of $FeCl_2$·$4H_2O$, 3 mmol (0.3329 g) of SeO_2) was mixed with 1 mmol of HF (0.4 ml) and 0.7mL of deionized water. $RbFe_3(SeO_3)_2F_6$: Hexagonal plate-like single crystals were obtained from the similar hydrothermal reactions using a mixture of RbOH / $FeCl_2$•$4H_2O$ /SeO_2 with the molar ratio of 1.6:1:3 (1.6 mmol of RbOH (0.15 ml), 1 mmol (0.1988 g) of $FeCl_2$·$4H_2O$, 3 mmol (0.3329 g) of SeO_2) and 1.1 mmol of HF (0.4 ml), 0.8mL of deionized water).

[a] School of Environmental & Chemical Engineering, Jiangsu University of Science and Technology, Zhenjiang 212003, Jiangsu, Perople's Republic of China.
[b] Université Lille Nord de France, UMR 8181 CNRS, Unité de Catalyse et de Chimie du Solide (UCCS USTL), F-59655 Villeneuve d'Ascq, France.
[c] Institut Laue-Langevin, Avenue des Martyrs 71, Grenoble Cedex, France
†Email: m.f.lv@hotmail.com, *Email:olivier.mentre@univ-lille.fr
Electronic Supplementary Information (ESI) available: See DOI: 10.1039/x0xx00000x

Please do not adjust margins

Each mixture was transferred into a stainless-steel autoclave (23 mL) with a Teflon liner, and was heated to 220 °C for 72 hours and cooled down to room temperature with a rate of 2.5 °C/h. The products were recovered by filtration and rinsed thoroughly with water.

Characterization

The single crystal XRD (SCXRD) data of reported materials have been collected using a Bruker SMART APEX II. The diffraction data at room temperature were obtained via a narrow-frame method with scan widths of 0.30° in ω and an exposure time of 10 s/frame. The program SAINT [4] was used for integration of the the diffraction profiles. The intensities of the obtained data were amended for air absorption, polarization, Lorentz factor etc. Semi-empirical absorption corrections were applied using the program SADABS. [5] The data collection and pertinent data of the refinements for $AFe_3(SeO_3)_2F_6$ (A=K, Rb) are summarized in Table 1. Deposition number CCDC 2086420, 2086421 for $KFe_3(SeO_3)_2F_6$ and $RbFe_3(SeO_3)_2F_6$, respectively. The refined anisotropic displacement parameters and atomic coordinates are summarized in the supplementary information (SI Table S1,S2, S4, S5).

Powder XRD (PXRD) patterns were collected using a Bruker D8 Advance X-ray powder diffractometer with Cu-Kα radiation (λ = 1.54056 Å, 40 kV/40 mA). The XRD powder patterns shown in Figure S1, S2, match well the calculated patterns using the model obtained from the single crystal data reported.

*SEM/*EDX of the isolated transparent crystals was carried out to determine approximate ratios of elements using a Phenom ProX desktop analyzer for the reported materials. Semi-quantitative EDX for $AFe_3(SeO_3)_2F_6$ (A=K, Rb) reveal A:Se:Fe:F ratios of 1.03:2.28:3.15:5.28 (K) and 1.27:2.20:3.03:5.84 (Rb) respectively (Figure S3, S4) approaching the refined stoichiometry.

Infrared spectra of the reported materials were recorded on a Varian 670-IR FTIR spectrometer in the 400−4000 cm^{-1} spectral range, with the well ground samples intimately contacted by an *attenuated total reflection (ATR) accessory* (Figure S5). It shows the absence of any hydroxyde groups in the prepared samples. TGA experiments was performed using a *thermal* gravimetric *analyzer* (Model: TGA5500*, TA* Instruments). Powdered samples for the reported compounds were mounted in alumina crucibles and heated at a rate of 10 °C min^{-1} from room temperature to 800 °C under flowing argon gas (Figure S6, S7).

The measurements of dc magnetic susceptibilities were conducted on a commercial Quantum Design Physical Properties Measurement System (DynaCool PPMS-9, Quantum Design) using VSM detection applying zero-field cooled (ZFC) and Field cooled (FC) cycles between 2 and 400K. A furnace was also used until 600 K. Isothermal magnetization curves were collected at the specified temperatures between 0 and 9 T. The specific heat measurements were performed using the heat capacity option of the PPMS.

Neutron powder diffraction data were collected on a 700 mg powder sample of $KFe_3(SeO_3)_2F_6$ on the high intensity powder diffractometer D20 at the Institut Laue Langevin (ILL), Grenoble, France. The sample was placed in a 5 mm Vanadium cylinder, cooled in a standard ILL Orange cryostat and measured at 1.5 K and 150 K using a wavelength of λ = 2.41 Å.

DFT+U calculations

DFT calculations were performed using the projector augmented-wave (PAW) method [6] implemented in the Vienna ab initio simulation package (VASP),[7] with the full-potential local-orbital scheme (FPLO9.00-33).[8] We used the generalized gradient approximation (GGA) for electron exchange and correlation corrections[9] applying the local density approximation (LDA) and LDA+U, U = 5 eV, for Fe atoms, this Hubbard term giving reliable magnetic parameters for Fe^{3+} oxides[10] (The cutoff energy for the plane wave expansion was 550 eV and reciprocal-space integration was performed on 8x8x2 k-points Monkhorst–Pack meshes. For the calculations of the magnetic exchanges identified in the plain text, we mapped the total energies for a number of collinear spin configurations onto a classical Heisenberg model, see Figure S8, to yield individual exchange couplings.

Table 1 Crystal data, measurement and structural refinement parameters of $AFe_3(SeO_3)_2F_6$ (A=K, Rb and Cs).

	$KFe_3(SeO_3)_2F_6$	$RbFe_3(SeO_3)_2F_6$	$CsFe_3(SeO_3)_2F_6$[3]
Molar weight (g/mol)	574.5	620.9	668.38
Symmetry	trigonal	trigonal	trigonal
Space group	*P -3 m 1*	*P -3 m 1*	*P -3 m 1*
Z	1	1	1
a (Å)	5.4261(2)	5.4478(2)	5.459(2)
c (Å)	9.9929(4)	10.1584(3)	10.537(3)
V (Å³)	254.799(17)	261.095(16)	271.9(2)
T(K)	293	293	296
μ (mm^{-1})	11.87	15.816	
R(int) (%)	4.95	6.83	
indep all (I > 3σ(I))	288	293	
indep obsd (I > 3σ(I))	246	232	
Numb. of refined parameters	17	17	
R(F) [*I* > 3σ(*I*)/all data, %]	3.37/4.57	3.31/4.33	
$R_w(F^2)$ [*I* > 3σ(*I*)/all data, %]	4.20/4.32	3.50/3.62	
$\Delta\rho_{max}/\Delta\rho_{min}$ (e /Å³)	1.27/-1.27	0.71/-1.03	

Results and discussion

The two reported compounds $AFe_3(SeO_3)_2F_6$ (A= K, and Rb) are perfect structural analogues to the A= Cs compound.[3] The full series adopt the trigonal centrosymmetric space group, *P-3m1*. In few words, there is one unique alkali metal site, one unique Se site, but two distinct Fe sites. Main crystal and bond distances and Bond valence sum (BVS) calculations [11] for the three compounds are given in Table S7, which confirmed Fe^{3+} and Se^{4+} oxidation states.

The crystal structure consists of AO_{12} polyhedra, FeF_6 and *trans*-FeO_3F_3 octahedra sharing their F corners while the pending oxygen belong to SeO_3 groups in trigonal pyramidal geometries, as shown in Figure 1a. The structure of $AFe_3(SeO_3)_2F_6$ consists of two-dimensional $[Fe_3(SeO_3)_2F_6]^-$ 3-octahedra thick layers, previously assigned to cubic tiles, and isolated by A^+ cations. Each layer contains three Fe sublayers, capped with SeO_3 linkers whereas the lone pairs on the SeO_3 point out towards their interiors. Figure 1a highlights the conservation of nearly unchanged layers while mainly the interleave

This journal is © The Royal Society of Chemistry 20xx

Please do not adjust margins

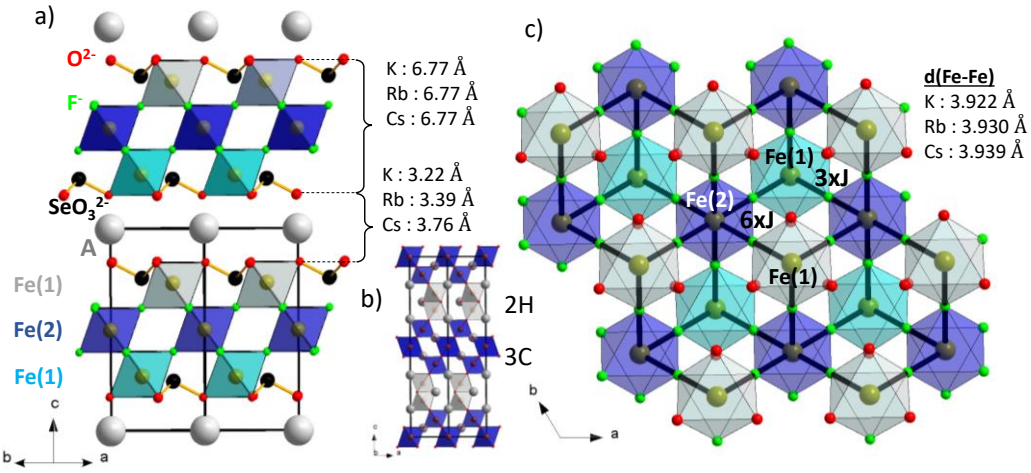

Figure 1 a) Cube tile lattice of $AFe_3(SeO_3)_2F_6$ (A= Cs, Rb, K, etc) along the [110] direction, $[Fe(2)F_6]$ octahedra are drawn in dark blue, $[Fe(1)O_3F_3]$ octahedra are highlighted in pale blue and grey.b) Evidence of similar three-octahedra-thick blocks in the 10 H $(ccccch)_2$ $Ba_5W_3Li_2O_{15}$. c) 2D $[Fe_3(SeO_3)_2F_6]^-$ block along the[00-1] axis with the tile-backbone and Js exchanges.

space filled by A^+ varies along the K, Rb, Cs series with respect to the *c*-lattice parameter elongation. Typical distances are given for A=K as follows: the equidistant Fe(2)−F bond lengths are 1.919(3) Å with the F−Fe(2)−F bond angles of 89.76(12)-90.24(10)°. In the slightly distorted $[Fe(1)O_3F_3]$ unit, Fe(1)−F and Fe(1)−O distances are 2.005(3) and 1.933(3) Å, respectively with O/F−Fe(1)−O/F bond angles of 85.35(12)-94.50(15)°(see Table S3).

As discussed in ref.[3] such isolated cubic-tiling lattices were never reported in the perovskite-based structural series such as Ruddlesden-Popper, Dion-Jacobson, Aurivillius etc, because they generally do not result from stacking along the [111] direction of the cubic-protype. However, such octahedral connectivity exists as 3C fragments of some hexagonal perovskites after removal of the face sharing octahedra, such as in the 10 H $(ccccch)_2$ $Ba_5W_3Li_2O_{15}$ where the cubic-tile contains both diamagnetic Li^+ and W^{6+} cations [12], see Figure 1b. In $AFe_3(SeO_3)_2F_6$, Fe(2) is connected to six Fe(1) and Fe(1) is connected to three Fe(2) through Fe(2)-F-Fe(1) super-exchanges (from Fe-Fe ~3.92 Å $_{K\text{-case}}$-to 3.94 Å $_{Cs\text{-case}}$, Fe-F-Fe ~178°) expected to be significantly antiferromagnetic, see Figure 1c. The competing Fe(2)-F-F-Fe(2) and Fe(1)-F-F-Fe(1) super-exchanges mediated across F-F contacts of ~2.72Å are expected to be weak compared to the linear Fe(2)-F-Fe(1) super-exchanges, despite Fe-F-F-Fe dihedral angles close to 0°(see Figure S9).

It is worth recalling the main magnetic properties reported for A=Cs in the preliminary work.[3] This compound was announced to order antiferromagnetically below T_N ~ 130 K. The dominating AFM Fe(2)-F-Fe(1) super-exchanges suggests FI arrangements between the three layers of the 2D-cube lattices, in a staggered manner [Fe(1)↑-Fe(2)↓-Fe(1)↑] leaving a net moment per block of approximately 1/3rd of its saturated value. A Curie-Weiss law was not established even well above T_N , i.e ~400K, which suggests strong magnetic exchanges inside the 2D-blocks. Below T_N a metamagnetic transition was announced from M(H) plots at ~0.05 T, typical of the

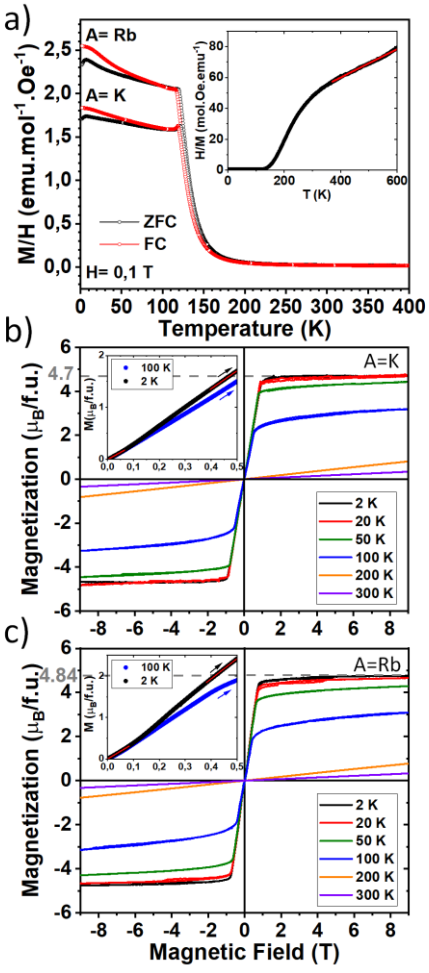

Figure 2 (a) FC and ZFC χ(T) plots for $AFe_3(SeO_3)_2F_6$ (A=K, Rb) in a magnetic field of 0.1T between 2 and 400K, (inset) 1/χ(T) plot for $KFe_3(SeO_3)_2F_6$ at 0.1T .The red solid line shows the Curie-Weiss fit between 380 and 600K . Field dependence of Magnetization for $AFe_3(SeO_3)_2F_6$ (A=K(b), Rb(c)) at various temperatures, the insets shows M(H) inflexion in the low field region.

Please do not adjust margins

breaking of AFM exchanges between the individual-blocks returning a 1/3rd magnetization plateau (M~5.2 μ_B/f.u.) as expected for the easy alignment of the individual block-FI net moments. An antiferromagnetic structure with spins lying in the (*a,b*) plane was proposed.

For A =K and Rb, the thermal dependence of the magnetic susceptibility χ(T) for H= 1000 Oe, is shown in Figure 2a with a evidence of a significant ZFC/FC divergence below the sharp transition at ~120 K in both cases.

A poor linearization of χ^{-1}(T) up to 400 K was observed for A=K and Rb, reminiscent of the A=Cs case.[3] In fact, a reliable $\chi = C/(T-\theta_{CW})$ Curie-Weiss fit was achieved only between 380 and 550 K. Above this temperature Fe3+ may initiate reduction in dynamical vacuum. It returns μ_{eff} = 5.40(1) μ_B per Fe^{3+} slightly lower than the expected spin-only value of 5.92 μ_B for high-spin Fe^{3+} and θ_{CW} = -337 (1) K. Using the mean-field (MF) model, $\theta_{CW} = zJS(S+1)/3k_B$, where *z=4* is the average number of neighboring Fe spins taking in consideration the predominant Fe(1)-F-Fe(2) super-exchanges only, yields antiferromagnetic $J_{MF}/k_B \approx$ -29 K for S = 5/2. Although this value should be considered with precaution, dealing with the high-temperature susceptibility setup, they comfort the occurrence of strong low-dimensional magnetic correlations, well above room-temperature.

Although slight, the divergence between ZFC and FC validates the development of a net magnetic contribution increasing with the field. This field-induced FI state is well evidenced by isothermal M(H) plots shown in Figure 2b,2c,S10. The maximal magnetization drastically depends on the temperature. At 2K it reaches 4.70 and 4.84 μ_B/f.u. at 9 T for A=K and Rb, respectively, nearly reaching the "ferrimagnetic" 1/3rd of the saturated magnetization. As shown in the insets of Figure 2b,2c, the metamagnetic transition is pronounced around $\mu_0 H$ = 0.2T at 2K for both the K and Cs analogs. It is reversible between the different M(H) branches. This behavior denotes a fragile AFM ground state already in the low field region.

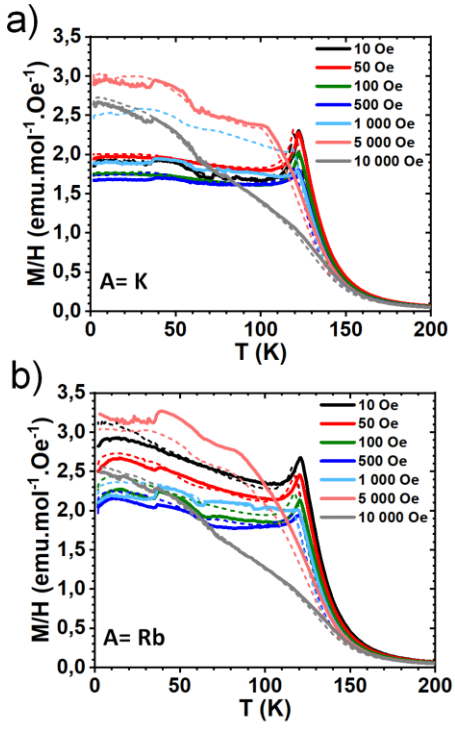

Figure 3 ZFC (dotted-lines) and FC (full-lines) magnetic susceptibility of $AFe_3(SeO_3)_2F_6$ (A=K(a), Rb(b)) under different magnetic fields between 2 and 200K.

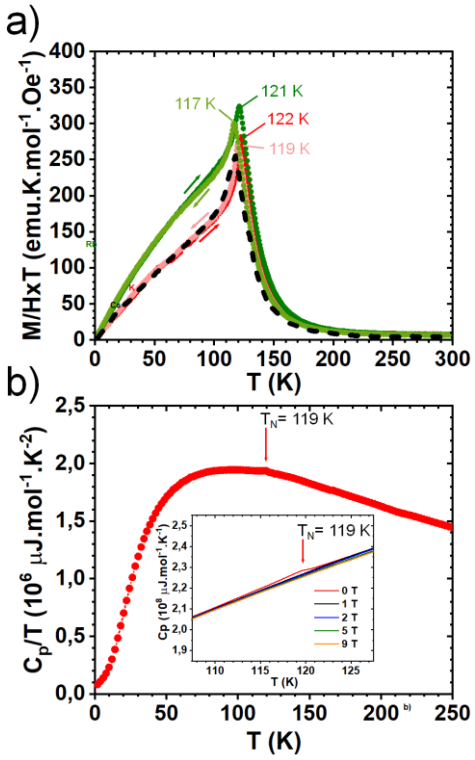

Figure 4 (a)χ(T)T vs. T curve for $AFe_3(SeO_3)_2F_6$ (A= Cs (reference 3), Rb, K) at 10 Oe.(b) The temperature dependence of Cp/T under 0T for $KFe_3(SeO_3)_2F_6$.The inset shows the temperature dependence of Cp under different magnetic fields.

Below T_N, the M/H (T) plots for A= K and Rb depend on the field values, see Figure 3. Below ~ 0.1 T, they are nearly constant below the sharp T_N peak. At higher fields, the T_N peak progressively vanishes and M/H(T) smoothly increases on cooling until it reaches a "noisy" transitory regime. This latter is assigned to the relaxation of the 2D magnetic domains under the field, with marked ZFC/FC divergences.

The Neel temperatures can be roughly estimated from the sharp maxima in the thermal dependence of the product χT at low field, e.g. 10 Oe, followed by a subsequent drop. Even at such low field the maxima depend on the sample magnetic history and hysteretic $\chi T(T)$ peaks are observed in ZFC/FC sequences, well understood by a 1st order magnetic transition. We found the maxima at $T_N(K)$ ~$119_{cooling}$-$122_{warming}$, $117_{cooling}$-$120_{warming}$ K and ~$117_{warming}$ for A=K, Rb, Cs [3] respectively, as shown on the Figure 4a. It coincides with the weak kink in C_p and C_p/T at 119 K observed for A=K on cooling (Figure 4b), supporting the occurrence of a thermodynamic magnetic transition with poor contribution to the magnetic entropy at T_N due to strong magnetic exchanges in-plane. The C_p peak rapidly vanishes under magnetic field, see the inset of the Figure 4b. It follows a singular situation above the metamagnetic transition which, at this stage resembles to a field-aligned paramagnet. C_p under zero field and 1T are shown on Figure S11 for A=K and Rb. For comparison, standard behaviors along both spin-flip and spin-flop transitions preserve the

This journal is © The Royal Society of Chemistry 20xx

Please do not adjust margins

Please do not adjust margins

C_p lambda-type anomalies at T_N at relatively high field, see recent cobalt arsenates compounds.[13] Hence, our data suggest the loss of uniaxial spins together with a relatively weak magneto-crystalline under applied field. It is noteworthy that the experimental T_N values are very similar (~120 K) for all compounds, a counter-intuitive behavior if one considers the expected variation of the Fe-Fe spin-exchanges (SEs) across the [Alkali] interleaves with a versatile size, see Figure 1a. Indeed, the shortest super-super exchanges Fe-O-O-Fe (J_{inter}) paths between two next blocks along *c* involve Fe-Fe/O-O distances of 6.13/3.22 Å (A=K), 6.29/3.39 Å (A=Rb) and 6.61/3.76 Å (A=Cs), with O-O separations much above the sum of the oxygen Van der Waals radii. Such features refute the setting of significant AFM interactions by SEs, especially around T_N~120 K, a rather high ordering temperature. Indeed, SEs are more generally short-ranged (dropping exponentially with inter-spin distance in ferromagnetic insulators for instance). However, the situation resembles the high T_N 3D-antiferromagnetic ordering of some cuprate-related superconductors such as $(Ca_{0.85}Sr_{0.15})CuO_2$ with high T_N=537(5) K. It results from the crossover from large intraplanar spin-spin correlations at high temperature to a 3D ground state driven by very weak out-of-plane couplings (J_{inter}/J_{intra} = 0.016) between Cu^{2+} ions .[14] The Néel Temperature of such Quasi-Low-Dimensional Heisenberg antiferromagnets was rationalized by Quantum Monte-Carlo (QMC) simulations giving empirical formulas describing T_N for a wide range of exchange ratio [15]. This point will be discussed later on the light of the refined magnetic structure and calculated exchange values.

The magnetic structure of $KFe_3(SeO_3)_2F_6$ at zero field was solved and refined from NPD data collected at 1.5K on the D20 diffractometer (λ=2.41Å) at the Institut Laue Langevin (ILL), Grenoble, France. The magnetic contributions growing below T_N can be indexed with the magnetic propagation vector *k*= [0,0, ½]. The magnetic symmetry analysis performed using Basireps[16] indicates a decomposition of the Γ magnetic representation into four irreducible representations ($\Gamma_{1\text{-}4}$) of dimension 1 and two ($\Gamma_{5\text{-}6}$) of dimension 2. For Fe(2), the decomposition yields $1\Gamma_3 + 1\Gamma_6$, but $1\Gamma_2+1\Gamma_3+1\Gamma_5+1\Gamma_6$ for Fe(1). The representation Γ_6 for both sites leads to the best agreement, which involves *in-plane* components only with spins parallel to [110] or trigonally-equivalent directions, see Table 2. Within isolated blocks, the two bordering Fe1 sites are parallel, but antiparallel to Fe2. R_{magn} was significantly improved from 6.94% to 6.28% relaxing individual Fe1 and Fe2 moments with a better matching of most of the magnetic satellites. It returns M_{Fe1} =3.72(3)μ_B and M_{Fe2}=4.25(5)μ_B . We note the presence of preferred orientations mainly occurring along [001] related to the hexagonal-crystallite shape. They have been refined on the data collected at 150 K using the March-Dollase function and applied on the data collected at 1.5K. However, it does not perfectly correct the nuclear profile, as shown on the Figure 5, plausibly due to multi-directional preferred orientations. In essence, our refined magnetic structure matches rather well earlier prediction for A=Cs. [3] The spin structure is compatible with a 3D-*XY* model, with the coupling between the layers hold by either weak J_{inter} exchanges or by spin-anisotropy able to freeze the magnetic moments in specific directions.

To unravel this point, single crystals of $KFe_3(SeO_3)_2F_6$ have been

Table 2 *Mx*,*My*, *Mz* according to the Γ6 irreducible representation for the magnetic structures of $KFe_3F_6(SeO_3)_2$compounds.

coordinates	Γ6 : *Mx, My, Mz*	$M_{total}(\mu_B)$
Fe(1) : *x,y,z*	-2.15(2), -2.15(2), 0	-3.72(3)
y,x,-z	-2.15(2), -2.15(2), 0	-3.72(3)
Fe(2) : *x,y,z*	2.45(3), 2.45(3), 0	4.25(5)

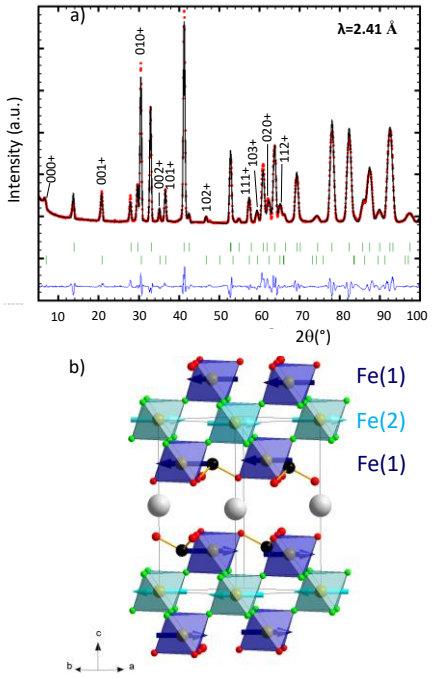

Figure 5 a) PND Rietveld refined patterns at 1.5 K and b) refined magnetic models for $KFe_3(SeO_3)_2F_6$.

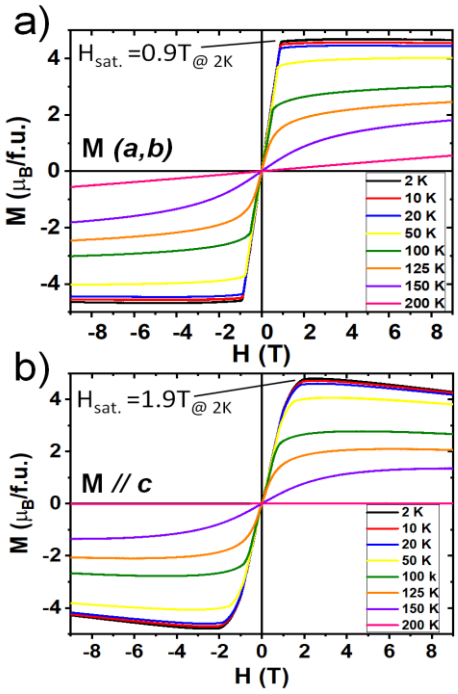

Figure 6 M(H) curves of single crystals of $KFe_3(SeO_3)_2F_6$ in-plane (a) and parallel to the c-axis(b).

Please do not adjust margins

Please do not adjust margins

aligned in epoxy resin at room temperature under an applied field of 9T. After drying, the observation of the crystals by transparency in the resin validates *in-plane* easy magnetic-axis active already in the paramagnetic domain, all of them being oriented with their *c*-axis normal to the field. The M(H) plots parallel and perpendicular to the *c-axis* are shown on Figure 6. They are very similar and both show the 1/3rd saturation plateau against a robust in-plane spin direction. It returns an easiest alignment in the (*a,b*) plane at low field, in good agreement with the refined magnetic structure. Note on the Figure 6, that the weak decrease of $M_{//c}$ after saturation is due to our not perfectly aligned sample. Above 20 KOe, the magnetization is nearly isotropic. In essence, when H is applied parallel to *c*, the moments rapidly flip following the field direction and $M_{//c}$ reaches the 1/3rd plateau. It comforts the robust FI topology within the layers hold by strong J_{intra} superexchanges, returning a net ~4.5μ_B/f.u moment. The anisotropy field H_{anis}, can be quantified by the field at which the magnetization perpendicular to the easy-axis saturates. However, for the title series, dealing with a AFM → FI metamagnetic transition, it sounds more realistic to consider H_{anis} as the ΔH difference to reach saturation between the two directions, i.e. ~1 KOe. This value is much weaker that what is found in several other 2D-compounds such as the layered ferromagnetic CrI_3 in bulk (H_{anis} ~19 KOe) with easy magnetic *c*-axis.[17,18] Despite very weak van der Waals inter-layer interactions in CrI_3 , the situation is different, the magnetic properties being thickness-dependent, with the crossover between a mean-field type interactions in the bulk (Tc =61K)[19] and an Ising 2D-regime for single flakes (Tc=45 K). [20] The results of our DFT+U calculations of the magnetic exchanges in the layer J_{intra} (= $J_{Fe1\text{-}F\text{-}Fe2}$) and between the blocks J_{inter} (=$J_{Fe1\text{-}O\text{-}O\text{-}Fe1}$) are listed for the three compounds in Table 3. It shows nearly constant J_{inter} (93-96 K) and J_{intra} (0.21-0.44 K) exchange values. Note that J_{intra} are found inversely scaled by the intermediate O---O distances, as expected. The very weak J_{intra}/J_{inter} ratio of ~3.10^{-3} validate a strongly anisotropic distribution of J's in our compounds. Phenomenologically the Fe^{3+} single-ion anisotropy , which even if expected very weak for (L=0) ions, mat also contribute to the spin-freezing at T_N, hampering significantly the spin fluctuations and participate to the AFM ordering between the layers.[21]

While genuinely 2D models cannot display long-range order (LRO) above zero temperature, apart the 2D-Ising exception (see $BaFe_2(PO_4)_2$ with *Tc* ~65 K [22], the weak estimated J_{inter} couplings, lead to a finite Néel temperature T_N [15]. The T_N dependence was analyzed by a modified random-phase approximation (RPA) giving the simple formula $T_N = 4\pi \cdot n \cdot J_{intra} / [b - \ln(J_{inter}/J_{intra})]$, with n and b constant estimated for S= ½ and S = 1. Besides the theory behind this empirical expression, it highlights the possibility for high ordering temperature, as verified in the $(Ca_{0.85}Sr_{0.15})CuO_2$ case mentioned above[14]. Using the parameters fitted for S=1 (n=0.68 and b=3.12) and the Js from DFT, we calculated the values listed in Table 3, and although underestimated (using parameters refined for S=1 Heisenberg spins), they show a correct correlation with the experimental results.

Here we discuss the ingredients governing the spin-structure below T_N and the easy spin-reversal of 2D-macrospins in an applied magnetic field. Besides the well-known influence on the spin orientations by spin-orbit coupling (SOC), spin-exchange (SE), magnetic dipole-dipole interactions (MDD), in the title series, the occurrence of AFM ordering around 120 K mediated by very weak exchanges across the alkali interleaves

Table 3 The magnetic exchanges calculated for $AFe_3(SeO_3)_2F_6$ (A= K, Rb, Cs) by DFT +U (U=5 eV) and experimental versus estimated T_N (see Ref.15), and calculated MDD.

Compound	A=K	A=Rb	A=Cs
J_{intra} / k_b (K)	96.0	94.6	93.0
J_{inter} /k_b (K)	0.64	0.44	0.21
T_N exp. (warming).	122	120	117
T_N calc. [15]	100.9	95.2	86.3
MDD (K) per Fe(1) Fe(1) → next block	-0.040	-0.038	-0.034

question about the relative role of the various ingredients at T_N. First, similarly to the layered $Sr_3Fe_2O_5$, [23] SOC being a single site interaction, it cannot determine the ordering between FI layers in the title series. Contrarily MDD are long-range multisite interactions, which are very weak between individual spins in an AFM state, but may become sizeable between 2D-macrospins, and may influence the orientation of the spins in the layers. For instance, MDD interactions are responsible for the formation of domains at high temperature in ferromagnets,[24] and strongly involved in the 3D magnetic ordering of highly separated layers in lamellar double hydroxides or chain systems.[25] MDD interactions are scaled by $1/r^3$ (where *r* is the interlayer distance given by the unit cell parameter *c*) and were estimated between the external Fe(1) and Fe(1), Fe(2) atoms of the next block in a sphere delimited by the cutoff distance Fe-Fe ≤ 12Å, which correspond to the sum of >40 individual contributions. We use the spin orientations from the refined magnetic structures and the following formula recently applied to $BaCoAs_2O_7$ multiferroics [26] for individual contributions:

$$\mathrm{MDD:H} = -\left(\frac{{\mu_B}^2}{{a_o}^3}\right)\left(\frac{a_o}{r_{jk}}\right)^3 \left[3\left(\overrightarrow{m_j}\cdot\overrightarrow{e_{jk}}\right)\left(\overrightarrow{m_k}\cdot\overrightarrow{e_{jk}}\right) - \overrightarrow{m_j}\cdot\overrightarrow{m_k}\right]$$

Where $\overrightarrow{m_{J,k}}$ are refined moments in μ_B. a_o is the Bohr radius (0.529177 Å). r_{jk} is the distance between the spin sites *j* and *k*. and $\overrightarrow{e_{jk}}$ is the unit vector along the intersite distance. ($\mu_B{}^2$/ $a_o{}^3$)= 0.181meV.

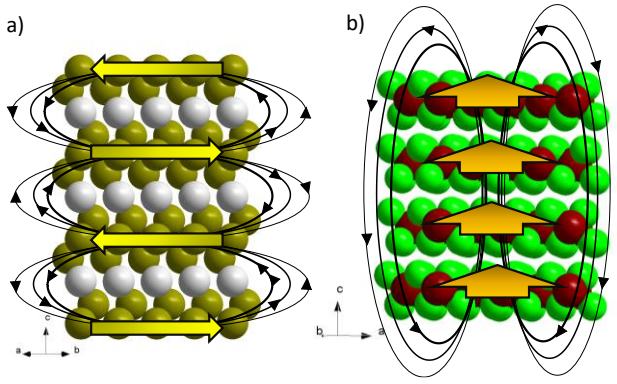

Figure 7 scheme of the MDD interactions, macrospins and idealized field lines for a) the AFM $AFe_3F_6(SeO_3)_2$ compounds (only greenish and grey spheres are represented for Fe and Ba atoms), b) the FM CrI_3 (brown and grey spheres are Cr and I atoms).

This journal is © The Royal Society of Chemistry 20xx

Please do not adjust margins

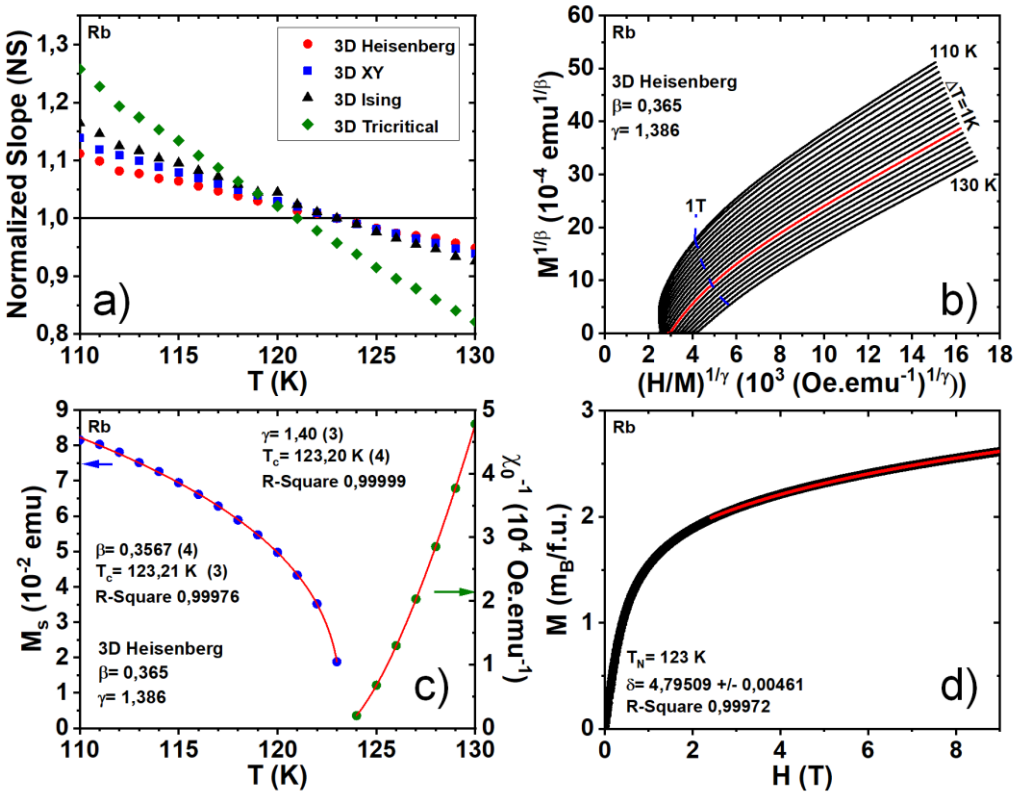

Figure 8(a) Temperature dependence of normalized slope (NS) for $RbFe_3F_6(SeO_3)_2$, (b)The isotherms of $M^{1/\beta}$ vs. $(H/M)^{1/\gamma}$ with parameters of 3D-Heisenberg model, (c) the M_S (left) and χ_0^{-1} (right) as a function of temperature for $RbFe_3F_6(SeO_3)_2$, (d)isothermal M(H) at T_C(all red solid curves are fitted).

Our results are listed in Table 3 and show negative (i.e. stabilizing) energies of around 10% of J_{inter} which cannot be neglected. It strongly suggests that the collective MDDs stabilize the antiferromagnetic in-plane spin ground state, see Figure 7a. In addition, taking the fragile spin alignment broken at H_c = 100 Oe at 2 K, one can estimate the energy to flip individual spins in a magnetic field, given as E= g.μ_B.*Hc*.S. We found E/K_b =0.03K meV, which is typically the order of magnitude of our calculated inter-layer MDD exchanges. In an antagonist manner, MDDs in a ferromagnetic order between weakly coupled ferromagnetic 2D units is favored by perpendicular spins and could be a plausible scenario for CrI_3 in its mean field regime (Tc=61K), i.e. above the temperature of 45K of the Ising setting, see Figure 7b.

All together, i) the contribution of MDDs and weak J_{inter} exchanges, ii) the Néel ordering at relatively high temperature, iii) the metamagnetic destabilization under field into a FI for any field direction, question about the critical behaviors at T_N but at high field. Clearly we aim to probe the critical exponents associated with the field induced transition into a ferrimagnetic state, and the validity of our analysis makes sense at finite field, while critical exponents of ferromagnets can be defined only in the limit of H=0 and T= Tc.

In that purpose, we have used the modified Arrott-plot treatment detailed for the 3D-$Cr_{11}Ge_9$,[27] 2D-CrI_3, [19] 2D-$CrGeTe_3$,[28] all of them displaying a relatively weak magneto-crystalline anisotropy with easy spin reversal perpendicular to the easy-magnetic axis under moderate magnetic field, similarly to the title-series. They allow to experimentally estimate the critical exponents from the data at finite H around Tc. In our case dealing with a low field spin flop-like transition, the validity of the Arrott-analysis, adapted to ferromagnets is questionable. However, if one assumes an effect of the low-field AFM ordering similar to the domain structure of an ideal ferromagnet, significant issues can be anticipated. For $RbFe_3F_6(SeO_3)_2$, the *M(H)* plots near T_c (interval ΔT=1K) are shown in Figure S12a after correction for the demagnetizing field, using the low-H magnetization. Generally, the critical exponents obey the Arrott-Noakes equation of states $M^{1/\beta} = A(T-T_C)+B(H/M)^{1/\gamma}$. [29] We first checked that the mean-field where β=1/2 and γ=1.0 [30] was not verified as M^2 vs. *H/M* should be a bunch of parallel lines, at least in the high field range, passing through the origin at T_c, see Figure S12b. Their positive slopes validate a 2nd order magnetic transition, but their downward curvature suggests the use of modified Arrott plots to extract realistic critical exponents, besides the mean-field model. The four plausible models in agreement with the refined 3D-ordering and the alignment of 2D-macrospins, namely the 3D-Heisenberg (β = 0.365, γ = 1.386), 3D-Ising (β = 0.325, γ = 1.24), tricritical mean-field (β = 0. 25, γ =1.0) and 3D-XY (β = 0.345, γ = 1.316), have been used, as shown in Figure S13. The most appropriate models returning parallel lines (with a slope $S(T) = dM^{1/\beta}/d(H/M)^{1/\gamma}$) was determined by calculating the deviation of the normalized slope $NS = S(T)/S(Tc)$ to 1. T_c is chosen for $M^{1/\beta}$ vs. $(H/M)^{1/\gamma}$ crossing the origin, i.e. around 121-123 K depending on the model and refined latter. *NS(T)* are plotted in Figure 8a, which returns the 3D-Heisenberg and 3D-XY as the best

Please do not adjust margins

ones. It discards the 3D-Ising case, which is inconsistent with the 2D-degeneracy of the refined magnetic structure. The 3D-tricritical model is also refuted, giving the worst agreement, contrarily to the $CrGeTe_3$ case, in which a 2D to 3D magnetic phase transition locates near a tricritical point. [28]

The theoretical β and γ values are poorly discriminating between the 3D-Heisenberg and XY models. However, keeping in mind that the critical temperature concerns the ordering between individual layers with intrinsic FI correlations much above T_N, the best-matching 3D-Heisenberg is relevant, assisted by i) the three-axial (*x,y,z*) components of anisotropic exchanges and the MDD interactions across the interblock gap. Using the plot of Figure 8b, the linear extrapolation from the high field region (between μ_0.H =3.6 and 9T , i.e. well above the AFM → FI deviation) to the intercepts with the axes $M^{1/\beta}$ below T_c returns reliable spontaneous magnetization *Ms(T,0)*, while their intercepts with the $(H/M)^{1/\gamma}$ above T_c returns $\chi_0^{-1}(T, 0)$, see figure 8c. Then T_c, β, and γ have been fitted to the critical exponents expressions, defined near T_c as [31]:

$$M_s(T) = M_0 ((T_c-T)/T_c)^{\beta} \quad T< T_c \quad (1)$$
$$H/M(T)=h_0/m_0((T-T_c)/T_c)^{\gamma} \quad T> T_c \quad (2)$$

It returns β=0.357(3), T_c=123.21(3)K in the low temperature region and γ=1.40(3), T_c =123.2(4) K in the high temperature region, close to theoretical values of the 3D-Heisenberg model (β=0.365, γ=1.386). Finally, the exponent δ defined at T_c by $M=DH^{1/\delta}$ was directly estimated from the critical isotherm at T_c, see Figure 8d. It yields δ =4.795(5) for H> 2.5 T, close to its theoretical value of 4.8. It nearly verifies the Widom scaling relation $\delta=1+\gamma/\beta$ giving 4.92 from our fits, which demonstrate the reliability of our set of critical exponents.

Conclusions

We report here the interactions between magnetic ions leading to a periodic lattice of 2D spin-clusters already at room temperature, themselves interacting in an antiferromagnet at T_N ~120 K, and so-mixing two different energy scales. There is a recent interest in materials straddling this spin/macrospin border because the interplay of different dimensionalities and interaction scales within and between clusters can lead to unusual physics, see for example, the formation of hexameric Cu_6 S=1 macrospins and their interactions in 2D-square lattices in $A_2Cu_3(SO_4)_3$ [32] or Cu_2OSeO_3 with a chiral lattice built by inner-Cu_4 tetrahedra which hosts several skyrmion phases.[33] However such magnetic systems are rarely achieved in real materials. In the $AFe_3F_6(SeO_3)_2$ family of compounds strong intralayer ferrimagnetic correlations are active up to 400 K, induced by strong Fe-F-Fe superexchanges between S=5/2 spins. The 2D-spin clusters order antiferromagnetically around T_N =120 K assisted by weak exchanges inter the layers (J_{inter} ~0.5K) in the whole series, where MDD interactions support their in-plane spin orientations as refined from NPD. It is striking that weak J_{inter}/J_{intra} of ~10^{-3} ratio generate a magnetic structure at so "high" temperatures. In an applied magnetic field, the robust 2D-ferrimagnetic spin-clusters progressively align to the external field, up to the 1/3rd magnetization ferrimagnetic-saturation. This 2nd order transition is associated with critical exponents suggesting a 3D Heisenberg topology,. Given, the relatively weak magnetic anisotropy deduced from M(*a*,*b*) and M//c measurements, the resulting spin configuration above H_c is expected directionless, forming a field induced paramagnet of 2D-macrospins in good agreement with the vanishing of the anomaly right above H_c and with respect to the relatively weak anisotropy field of ~12K Oe measured on single crystals at 2K.

Conflicts of interest

There are no conflicts to declare.

Acknowledgements

H. Y.,T. Z., X. Z., Y. J., and M.L. acknowledge support from the National Natural Science Foundation of China (Award No.21671185). O.M., acknowledge support from the ANR (Grant ANR-16-CE08-0023) and the FEDER Région Hauts-de-France, they also acknowledge the ILL for the allocated beamtime (DOI 10.5291/ILL-DATA.EASY-654) and the ILL Instrument Control Service for their support before and during the experiment. Finally dealing with mixed anion compounds, the JSPS Core-to-Core Program (A) Advanced Research Networks (JPJSCCA20200004) is also acknowledged as a source of motivation.

Notes and references

1 C. Mann, L. Asaro, J. Hyde, M. Jensen, T. Schroeder, *Discret. Math*., 2015, **338**, 10-22.
2 S. T. Bramwell, M. J. P. Gingras, *Science*, 2001, **294**, 1495-1501.
3 H. Lu, H. Kageyama, *Inorg. Chem*., 2018, **57**, 6186-6190.
4 SAINT, Area-Detector Integration Software, Siemens Industrial Automation, Inc., Madison, 1996.
5 SADABS, Area-Detector Absorption Correction, Siemens Industrial Automation, Inc., Madison, 1995.
6 P. E. Blöchl, *Phys. Rev. B*, 1994, **50**, 17953‑17979.
7 G. Kresse, M. Marsman, J. Furthmuller, Vienna Ab-initio Simulation Package (VASP). 2012.
8 K. Koepernik, H. Eschrig, *Phys. Rev. B*, 1999, **59**, 1743‑1757.
9 J.P. Perdew, K. Burke, M Ernzerhof, *Phys. Rev. Lett.*, 1996, **77**, 3865‑3868.
10 Y. Meng, X.-W. Liu, C.-F.Huo, W.-P. Guo, D.-B. Cao, Q. Peng, A. Dearden, X. Gonze, Y.Yang, J. Wang, H Jiao, Y. Li, X.-D. Wen,*J. Chem. Theory Comput.* 2016, 12, 10, 5132–5144.
11 N. E. Brese and M. O'Keeffe, *Acta Crystallogr*., 1991, **B47**, 192–197.
12 A. J. Jacobson, B. M. Collins, B. E. F. Fender, *Acta Cryst.,* 1974, **B30**, 816-819.
13 B. Leclercq, H. Kabbour, F. Damay, C. V. Colin, A. Pautrat, A. M. Arevalo-Lopez, O. Mentré. *Inorg. Chem*., 2019, **58**, 12609-12617.
14 D. Vaknin, E. Caignol, P. K. Davies, J. E. Fischer, D. C. Johnston, D. P. Goshorn, *Phys. Rev. B*, 1989, **39**, 9122.
15 C. Yasuda, S. Todo, K. Hukushima, F. Alet, M. Keller, H. Takayama, *Phys. Rev. Lett.*, 2005, **94**, 217201.
16 J. Rodriguez-Carvajal, *Physica* B., 1993, **55**, 192.
17 M. A. McGuire, H. Dixit, V. R. Cooper, B. C. Sales, *Chem. Mater*., 2015, **27**, 612−620.
18 J. M. Friedt, J. P. Sanchez, *J. phys. C. solid state phys.*, 1978, **11**, 3731.
19 Y. Liu, L.Wu, X. Tong, J. Li, J. Tao, Y. Zhu, C. Petrovic, *Scientific Reports*, 2019, **9**, 13599.

 This journal is © The Royal Society of Chemistry 20xx

Please do not adjust margins

Please do not adjust margins

20 B. Huang, G. Clark, E. Navarro-Moratalla, D.R. Klein, R. Cheng, K. L. Seyler, D.Zhong, E. Schmidgall, M. A. McGuire, D. H. Cobden, W. Yao, D. Xiao, P. Jarillo-Herrero, X. Xu, *Nature,* 2017, **546**, 270–273.
21 R. Skomski, A. Kashyap, J. Zhou, D. J.Sellmyer, *J. Appl. Phys.,* 2005, **97**, 10B302.
22 H. Kabbour, R. David, A. Pautrat, H.-J. Koo, M.-H. Whangbo, G. Andre, O. Mentre, *Angew. Chem.* 2012, **124**, 11915-11919.
23 M. N. Roberts, J. K. Nagle, J, G. Finden, N. R. Branda, M. O. Wolf, *Inorg. Chem*., 2009, **48**, 19-21.
24 N.W. Ashcroft, N. D. Mermin, *Solid State Physics*; Saunders College, Philadelphia, PA, 1976. 673-674.
25 S. Ostrovsky, W. Haase, M. Drillon, P. Panissod, *Phys.Rev. B*, 2001, **64**, 134418.
26 B. Leclercq. A. M.Arévalo-López, H. Kabbour, S.Daviero-Minaud, A. Pautrat, T. Basu, C.V. Colin, R.-R.Das, R. David, O. Mentré, *Adv. Quantum Technol.*, 2021 ,**4** 2000064.
27 H. Han, L. Zhang, X. Zhu, H. Du, M. Ge, L. Ling, L. Pi, C. Zhang, Y. Zhang, *Scientific Reports*, 2016, **6**, 39338.
28 G. T. Lin, H. L. Zhuang, X. Luo, B. J. Liu, F. C. Chen, J. Yan, Y. Sun, J. Zhou, W. J. Lu, P. Tong, *Physical Review B*, 2017, **95**, 245212.
29 A. Arrott, J. E. Noakes, *Phys. Rev. Lett*., 1967, **19**, 786.
30 S.N. Kaul, *J. Magn. Magn.Mater.*, 1985, **53**, 5-53.
31 M. E. Fisher, *Rep. Prog. Phys.*, 1967, **30**, 615-730.
32 D. Nekrasova, O. Alexander, A.Tsirlin, M. Colmont, O. Siidra, H. Vezin, O. Mentré. *Phys. Rev. B*, 2020, **102**, 184405.
33 A.Chacon. L. Heinen, M. Halder, A.Bauer, W. Simeth, S. Mühlbauer, H. Berger, M. Garst, A. Rosch, C. Pfleiderer, *Nat. Phys*., 2018, **14**, 936.

Graphical Abstract

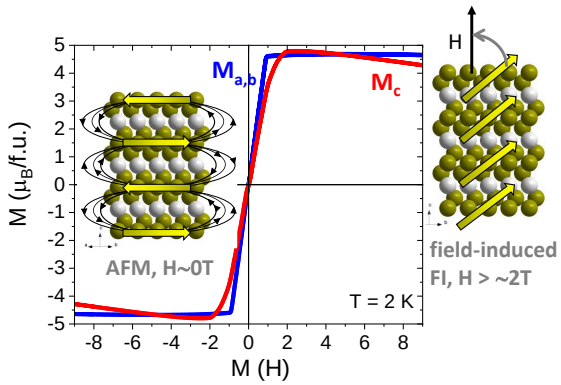

Weak magnetocrystalline anisotropy and breaking under field of the interlayer AFM exchanges in $AFe_3(SeO_3)_2F_6$ (A=K, Rb, Cs).

Please do not adjust margins